

Coulomb drag between carbon nanotube and graphene

Jean-Damien Pillet^{1,*}, Austin Cheng², Takashi Taniguchi³, Kenji Watanabe³, Philip Kim^{2,*}

¹*Department of Physics, Columbia University, New York, New York 10027, USA.*

²*Department of Physics, Harvard University, Cambridge, Massachusetts 02138, USA. and*

³*National Institute for Materials Science, Namiki 1-1, Ibaraki 305-0044, Japan.*

When two electrically isolated conductors are brought close, a current in one conductor can generate friction and drag electrons in the other via Coulomb interaction, thereby causing a charge imbalance in the dragged layer. This is known as Coulomb drag and has been used to investigate strongly correlated nature of low dimensional conductors [1]. Here, we report the observation of Coulomb drag between a two-dimensional electron gas in graphene and a one-dimensional wire composed of a carbon nanotube. We find that drag occurs when the bulk of graphene is conducting, but is strongly suppressed in the quantum Hall regime when magnetic field confines conducting electrons to the edges of graphene and far from the nanotube. Out-of-equilibrium measurements show that transitions between quantized charge states of the nanotube induce either strong suppression or enhancement of drag signal.

Due to geometrical reasons, drag effects [1] are particularly relevant for systems in which electrons are confined in one or two dimensions. Bilayers of two-dimensional (2D) electron gases separated by a few nanometers have been realized in semiconductor hetero-structures [2] leading to several groundbreaking experiments such as the observation of a super-fluid exciton condensate [3]: a quantum state carrying non-dissipative current of electron-hole pairs. Electrical devices based on hexagonal Boron Nitride (h-BN) encapsulated graphene [4] or bilayer-graphene [5, 6] has allowed the demonstration of Coulomb drag in 2D in previously inaccessible regimes and are subject of intense study motivated by the potential observation of a quantum condensate at much higher temperatures [7, 8]. In one-dimensional (1D) wires, Coulomb drag is also expected to reveal a rich variety of exotic phenomena such as the formation of interlocked charge-density wave [9] as well as Luttinger liquid behavior [10].

While in 2D the main observations of drag transport can be understood by assuming a weak Coulomb repulsion [11], this approach is believed to break down in 1D, where physics of electron is dominated by interaction. The limit of strong Coulomb repulsion is reached in devices showing larger confinement such as quasi-one-dimensional nanowires or in quantum dots [12]. For instance, electrostatically defined nanowires have shown

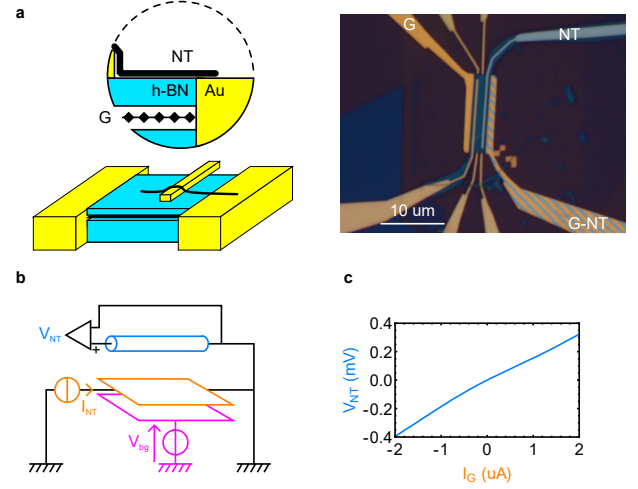


Figure 1. Description of the device and principle of the experiment. **a**, Schematic of the carbon nanotube-graphene device and optical image of the device with false color on electrodes connected to graphene (orange) and carbon nanotube (blue). The device is measured in a cryostat equipped with a superconducting coil that can generate magnetic field up to 9 T. **b**, Principle of Coulomb drag measurement across the nanotube. All measurements are performed using a 10 or 100 MΩ input impedance amplifier. **c**, Typical $V_{NT}(I_G)$ characteristic measured at temperature $T = 1.6$ K with $V_{bg} = 0$ applied on the back gate.

Coulomb drag signatures compatible with strongly interacting electrons such as negative drag [13] and diverging behavior at low temperatures [14]. In this work, we present electron drag measurements in an asymmetric system composed of a carbon nanotube and graphene where electrons are propagating in 1D and 2D respectively. This system of hybrid dimensions allows the study of Coulomb drag in unexplored regimes beyond what has been observed in conventional systems.

The device geometry used in this experiment is shown in Fig. 1a. A carbon nanotube is placed on top of an h-BN encapsulated graphene such that the carbon nanotube and graphene are electrically separated by a 12 nm thick h-BN. The device is made on an oxidized Silicon wafer that we use as a back gate. Both nanotube and graphene are connected to metallic electrodes and have a common electrical ground in order to minimize uncontrolled voltage fluctuations.

The principles of our experiment consist of flowing a current I_G through the graphene channel and detecting a

* jean-damien.pillet@college-de-france.fr;
pkim@physics.harvard.edu

voltage drop V_{NT} across the carbon nanotube (Fig. 1b). The slope of $V_{NT}(I_G)$ characteristics (Fig. 1c) provides the drag resistance $R_D = dV_{NT}/dI_G$. This drag resistance can be modulated by the voltage applied to the back gate V_{bg} reaching values of a few hundreds of Ohms. As illustrated in Fig. 2a, the role of graphene and carbon nanotube can be inverted, in which case the drag resistance is defined as $R_D = dV_G/dI_{NT}$ where V_G is the voltage drop across the graphene and I_{NT} the current flowing through the nanotube. In both cases, because the nanotube is four orders of magnitude smaller than graphene and because the nanotube is mostly sensitive to the current flowing in its vicinity, drag measurements provide local information on the graphene properties. And despite this physical asymmetry, we found that the values of R_D measured in both configurations are nearly identical due to the Onsager relation as we shall discuss below in detail.

Fig. 2b shows R_D as a function of V_{bg} when there is no applied magnetic field B . R_D shows a peak at $V_{bg} \approx 6$ V and saturates for high positive and negative gate voltages. No appreciable difference can be found between two different configurations of measurement described above. At first approximation, we expect a small effect of the back gate on the nanotube, since it is screened by graphene. We therefore interpret the peak in $R_D(V_{bg})$ as a manifestation of the density of states minimum in the linear band structure of graphene, close the Dirac point. It is informative to compare $R_D(V_{bg})$ with the gate dependent resistance of graphene $R_G(V_{bg})$ (inset of Fig. 2b). While the charge neutral Dirac point of graphene can be roughly identified around $V_{bg} \sim 10$ V, close to the peak position of $R_D(V_{bg})$, we note that, however, $R_G(V_{bg})$ exhibits a broader, asymmetric peak with a poorly defined maximum due to the charge inhomogeneity induced by the nanotube and to the local gating effect on the graphene channel coming from the nanotube contacts that are placed on top of h-BN. In contrast, our drag measurements are local and therefore insensitive to such disorder. We also note that the sign of R_D remains positive in the entire gate range where the type of carriers in graphene changes from electron to hole across the Dirac point [15]. One possible scenario is that the drag charge imbalance we observe is caused by energy transfer between nanotube and graphene rather than momentum drag [16].

The evolution of R_D with temperature is a good indicator to identify the relevant microscopic contributions. As seen in Fig. 2c, away from the Dirac peak, the signal first decreases with temperature T and then experiences a fast upturn with variations of approximately 25 percent, while at the Dirac peak, $R_D(T)$ increases continuously and seems to diverge when T approaches 0. These observations are in a sharp contrast with the conventional drag in 2D conductors where drag resistance follows a T^2 law [4]. The conventional theoretical description of 2D drag is often based on a lowest order perturbation on the interaction strength [1], and thus may not be applicable

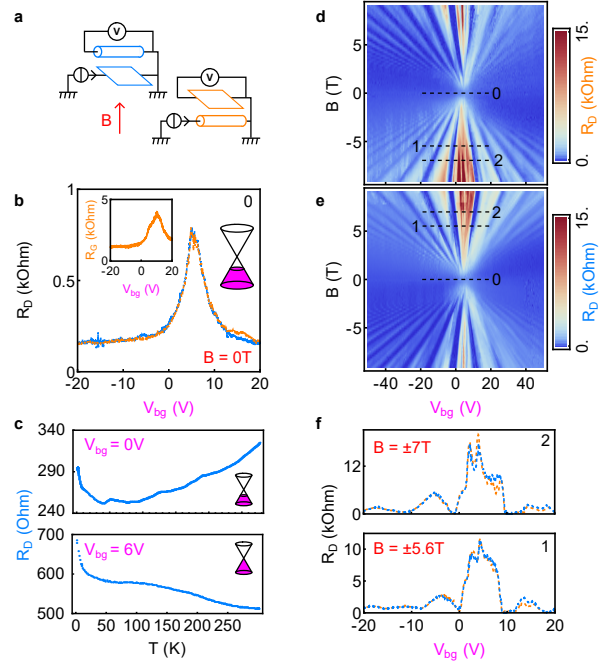


Figure 2. Drag response. **a**, Schematic diagrams for two different configurations of drag measurements. The arrow indicates the direction of magnetic field B . **b**, Measurements of R_D as a function of back gate voltage V_{bg} in absence of magnetic field. Left inset shows the resistance of graphene and right inset symbolizes the partially filled linear band structure of graphene. For the curve in blue, the drive current is flowing through the graphene and the voltage is detected across the nanotube. The orange curve shows similar drag measurement, the role of nanotube and graphene being inverted. **c**, Evolution of R_D with temperature T for $V_{bg} = 0$ V (top, corresponding to hole doped graphene as shown in the inset) and 6 V (bottom, corresponding to the Dirac point as shown in the inset). **d-e**, R_D measured as a function of V_{bg} and B in the two configurations pictured in schematic diagrams in **a**. We observe the formation of Landau levels when $B = \hbar\pi C_{SiO_2}(V_{bg} - V_{bg}^0)/2e^2N$ where \hbar is the reduced Planck constant, e is the charge of electron, N is an integer corresponding to the index of the Landau levels, V_{bg}^0 is the position of the Dirac peak and C_{SiO_2} is the capacitance per surface unit between the back gate and graphene. The horizontal dashed lines represent the cuts shown in **b** and **f**. **f**, R_D measured along the dashed lines shown in **d** and **e** at two different magnetic fields.

to our experiment, where strong Coulomb repulsion is expected due to confinement of electrons in the nanotube. And even though devices of hybrid dimensions such as ours have rarely been considered in the literature [17], it is known that higher order terms calculated for 2D conductors gives to R_D non-vanishing contributions at low temperatures [18], resulting in a non-monotonic evolution with temperature. Beyond perturbation, the Luttinger liquid theory also predicts a strongly non-monotonic behavior of R_D that largely depends on the microscopic details of the system [9, 10, 19–21].

Upon a finite magnetic field B applied perpendicular

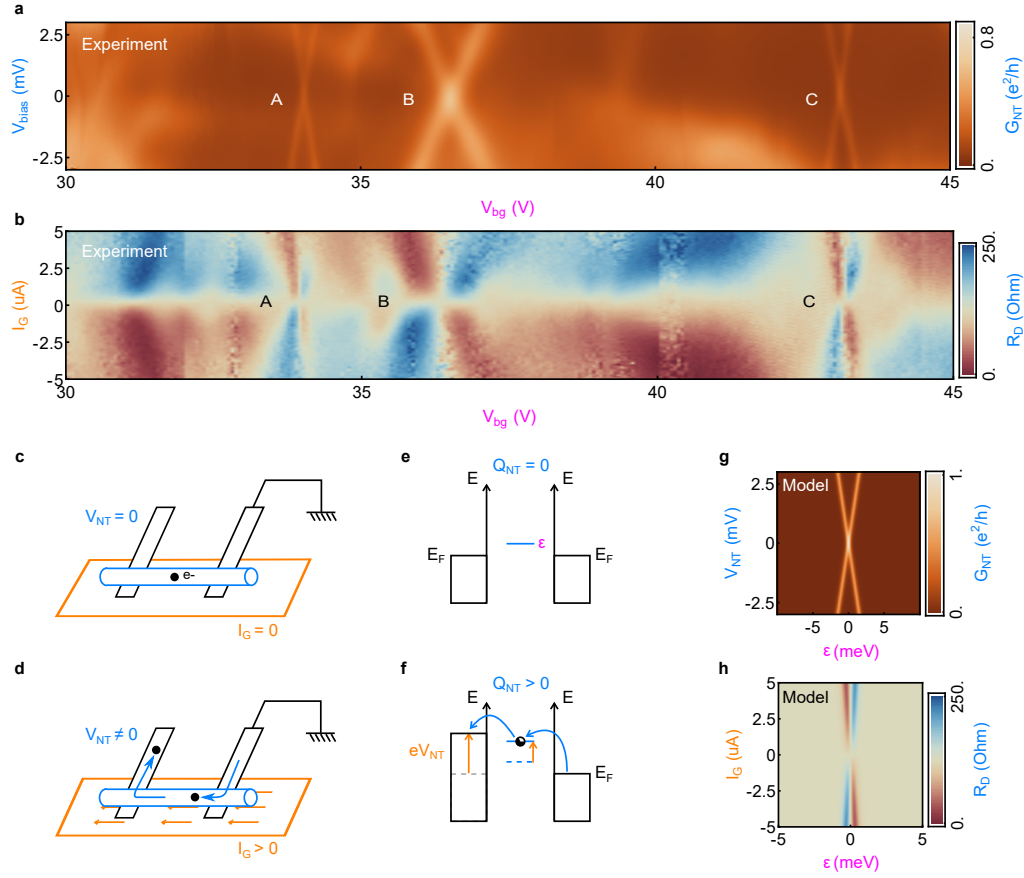


Figure 3. Out-of-equilibrium measurements. **a**, Conductance of the nanotube G_{NT} measured as a function of the voltage V_{bias} applied across it in a range of back gate voltage V_{bg} where graphene is highly doped and the effect of back gate on the nanotube is weak. No current is flowing through graphene. **b**, Drag resistance R_D measured across the nanotube as a function of V_{bg} and a finite DC current I_G flowing through graphene. White color corresponds to median values of R_D in the zero-bias limit, while blue and red respectively show increase and decrease of the drag resistance. **c**, When no current is flowing through the graphene channel, charges are localized in the nanotube and no voltage develops across it. **d**, If a current is flowing, charges are displaced by an effective friction and V_{NT} becomes finite. **e**, If one considers a single empty electronic level of the nanotube with energy ϵ , then a drag voltage developing across the nanotube changes the occupancy of this level. The energy cost associated to this process affects the magnitude of the drag signal. **g**, Simulated conductance of the nanotube by solving master equations for $I_G = 0$ as a function of the bias V_{NT} and ϵ . In our experiment ϵ can be controlled by V_{bg} . **h**, Simulated drag resistance R_D by solving the master equation for finite I_G to obtain the derivative dV_{NT}/dI_G . The temperature is chosen to be 1.6 K and the capacitance of the nanotube which control the amplitude of charge fluctuations around 100 aF.

to the graphene plane, we find that R_D develops a rich structure as a function of B and V_{bg} as shown in Fig. 2d and e. Similar to the Landau fan shown in R_G (supplementary Fig. S5), R_D exhibits a series of oscillations that disperse with magnetic field and back gate voltage, fanning out in the B - V_{bg} plane. In particular, we notice that R_D is suppressed to nearly zero when the Fermi level of graphene is in between Landau levels. In this quantum Hall (QH) state of graphene, the electronic bulk of graphene become incompressible and currents are carried at edges of the graphene channel. We find that R_D decreases by up to three orders of magnitude as graphene enters the QH regime from more than 10k Ω to only a few Ohms. This large modulation in R_D is understandable if we consider the distance between the nanotube

and the current: the nanotube is only 12 nm away from the current path when the bulk is conducting, whereas the distance becomes a few microns when the current is flowing along the edges.

One important finding is that R_D is not symmetric with the sign change of B , regardless of whether R_D is measured across the nanotube or graphene, as can be seen in Fig. 2d and e. For a circuit with two terminals, this symmetry should be preserved as it would otherwise violate time-reversal symmetry (see Supplementary). This apparent violation is due to the multi-terminal measurement configuration of our drag experiments. Even when no current is flowing through the nanotube, its electrons might scatter with those of graphene which induces finite non-diagonal terms in the conduc-

tance matrix relating currents and voltages in the device. In this case, time-reversal symmetry dictates that R_D should obey Onsager relations [22] implying $R_D^G(B) = R_D^{NT}(-B)$, where $R_D^{G(NT)}$ is the drag resistance measured across graphene (resp. nanotube). As illustrated in Fig. 2f, our measurements obey such relations and time-reversal symmetry is not violated in our experiment, even at low temperature, in contrast with what has been reported previously in devices based on two-dimensional conductors [23, 24].

The Onsager relations we confirm in the drag measurement only works in the linear response regime close to the equilibrium of the system. Away from this linear regime, we observe modulation of the drag resistance that is related to nanotube internal electronic structure. If we apply a voltage bias across the nanotube, this structure is apparent in conductance measurements (Fig. 3a) where we observe bright crosses (labeled A, B and C) corresponding to partial Coulomb diamonds revealing discrete electronic levels arising from spatial confinement as well as Coulomb repulsion. The smooth shape of these crosses suggests that conductance G_{NT} is dominated by a well-defined quantum dot but the uneven sizes of diamonds as well as the irregular background suggest a disordered environment. This structure also shows up in the drag resistance, when we drive the system out-of-equilibrium. Flowing a finite DC current in graphene I_G , we observe strong variations such that R_D can increase by two fold or be completely suppressed (Fig. 3b). Comparing Fig. 3a and b, we identify that a suppression occurs when a nanotube electronic level is aligned with the Fermi level of the grounded electrode, while enhancement occurs when it is aligned with the Fermi level of the floating one.

The observed correlations between R_D and G_{NT} in the out-of-equilibrium regime can be described by a phenomenological model based on a friction force $\vec{F}_f = \eta n_G \vec{v}_G$ that graphene current exerts on the localized electrons in the nanotube, where η is the friction coefficient, n_G is the graphene carrier density and v_G is the velocity of electrons in graphene. We introduce an effective friction coefficient η_{eff} , such that this force can be simply written as $F_f = \eta_{eff} I_G$. When I_G is finite, it displaces charges (see Fig 3c and d) across the nanotube from the grounded electrode to the floating one which has a potential V_{NT} that will consequentially increase. During this process, each charge acquires an energy $-eV_{NT} + \eta_{eff} I_G L_{NT}$ where the first term comes from electrostatics and the second term is the work of the friction along the length of the nanotube L_{NT} . As a small fraction of the displaced charges does not reach the electrode and remains in the nanotube (Fig. 3e and f), some of the friction work is converted to increase nanotube occupancy which suppresses the drag. Similarly charging energy can be released to favor the transfer of charge and enhance R_D . A more quantitative analysis can be done by employing a master equation formalism (see supplementary information). Fig. 3g and h show the simulated G_{NT} and R_D respectively, across a single res-

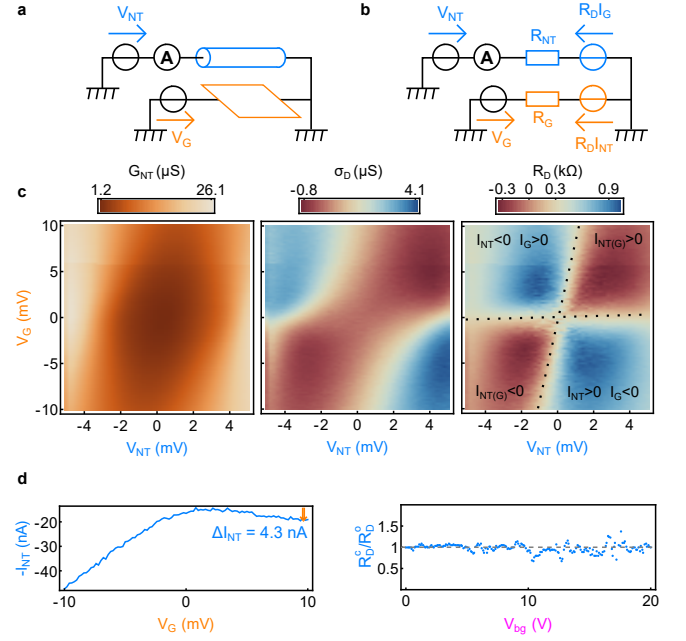


Figure 4. Non-linear drag response. **a**, Principle of simultaneous measurement of G_{NT} and R_D . Different frequencies are used for V_{NT} and V_G modulation to facilitate independent measurement. **b**, Schematic used for the lumped element circuit analysis. **c**, From left to right: differential conductance of the nanotube G_{NT} , drag conductance σ_D and drag resistance $R_D = \sigma_D R_{NT} R_G$ where $R_{NT(G)}$ are the resistance of the nanotube and graphene, respectively. We can distinguish four quadrants in R_D depending on the relative orientation of the current in graphene and nanotube. **d**, On the left: DC measurements of I_{NT} as a function of V_G with $V_{NT} = 3.2$ mV kept constant. The slope of the $I_{NT}(V_G)$ characteristic can change sign and the differential conductance σ_D can thus be positive or negative. On the right: ratio of the differential drag resistance measured at $V_G = 0$ across the nanotube in open circuit (Fig. 2a) and in closed circuit (schematic a) with $V_{NT} = 0$. These two different measurements yield consistent values.

onant level at energy ϵ , which can be tuned by V_{bg} in our experiment. While we do not reproduce the smoother variations of the background, both simulated G_{NT} and R_D exhibit the essential features that appear in the data across a single resonant level.

The unconventional sign of R_D , its temperature dependence and the variations induced by charge fluctuations suggest a non-conventional mechanism behind our observations possibly due to mesoscopic effects since the nanotube behaves as a quantum dot. Whether this mechanism is driven by charge repulsion [25, 26], quantum shot noise [27] or non-local cotunneling processes [28], the non-linearities in the nanotube conductance at a finite bias voltage can also produce non-linear drag behaviors. When both nanotube and graphene are biased separately as shown in Fig. 4(a), the current in the nanotube I_{NT} has two components: a standard resistive

contribution proportional to the nanotube conductance G_{NT} and a drag contribution proportional to R_D . Experimentally, we can distinguish these two contributions by frequency-division multiplexing with voltages having both a DC and an AC component. As shown in Fig. 4c at fixed gate voltage, the differential conductance of the nanotube $G_{NT} = dI_{NT}/dV_{NT}$ varies by more than one order of magnitude with V_{NT} , exhibiting a strong non-linear transport behavior but is weakly dependent on V_G . However, the drag conductance $\sigma_D = -dI_{NT}/dV_G$ varies rather strongly on V_G and V_{NT} . In this scheme, the non-linear drag resistance R_D can be related to σ_D through the relation: $\sigma_D \approx R_D/(R_{NT}R_G)$ (See Supplementary for derivation). The resulting drag resistance R_D show strong non-linear behavior including sign changes. In the right panel of Fig. 4c, R_D shows four quadrants separated by boundaries along which the system is in the linear regime (i.e., in the limit of vanishing I_{NT} and I_G) and R_D takes constant value. Note that if I_G and I_{NT} have opposite directions, R_D increases and stay positive but it decreases and reaches negative values for currents in the same direction. Such negative differential response, which can be explicitly demonstrated in DC measurement as well (Fig. 4d) could be of interest for the development of on-chip active devices.

METHODS

Supplementary information on methods of fabrication, analysis of Onsager relation, details of the phenomenological model used in Fig. 3g and h, as well as technical details about measurements and analysis used in Fig. 4 are available online.

Fabrication of the sample. We place a carbon nanotube on top of an h-BN encapsulated graphene by mechanical transfer. Metallic electrodes are designed with a standard e-beam lithography technique. The top surface of electrodes is covered with gold in order to avoid oxidation. The graphene is electrically connected using side contact technique, while other electrodes placed on the top h-BN layer are isolated from the graphene and are for contacting the carbon nanotube. We make sure before we incorporate the nanotube into the device that the parasitic tunneling between these electrodes and graphene

is completely negligible for the experiment, with tunnel resistance well above 1 G Ω . The nanotube, grown suspended over trenches by chemical vapor deposition, is then deposited by mechanical transfer onto the electrodes in the center of the graphene flake with $\sim \mu\text{m}$ precision (see Supplementary). For this step of nanofabrication, the device is entirely covered with an insulating layer of resist except for a small region of interest such that the carbon nanotube connects only the chosen electrodes. Prior to transfer, an optical characterization of the nanotube is performed using Rayleigh scattering in order to select metallic nanotubes that have no gap and conduct at all doping.

ADDITIONAL INFORMATION

Correspondence and requests for materials should be addressed to J.-D.P. or P.K.

ACKNOWLEDGMENTS

J.-D.P. would like to thanks Ç. Girit and C. Dean for fruitful discussions. This work is supported by ONR MURI N00014-16-1-2921 and Global Research Laboratory Program (2015K1A1A2033332) through the National Research Foundation of Korea (NRF) funded by the Ministry of science, ICT and Future Planning (MSIP). K.W. and T.T. acknowledge support from the Elemental Strategy Initiative conducted by the MEXT, Japan and JSPS KAKENHI Grant Numbers JP26248061, JP15K21722 and JP25106006.

AUTHORS CONTRIBUTION

J.-D.P. and P.K. conceived and designed the experiment. J.-D.P. and A.C. fabricated the samples and performed the measurements. J.-D.P. analyzed the data and wrote the paper. P.K. supervised the project. T.T. and K.W. provided the h-BN crystals.

COMPETING FINANCIAL INTERESTS

The authors declare no competing financial interests.

-
- [1] B. N. Narozhny and A. Levchenko, Coulomb drag. *Reviews of Modern Physics* **88**, 025003 (2016).
 - [2] T. J. Gramila, J. P. Eisenstein, A. H. MacDonald, L. N. Pfeiffer, and K. W. West, Mutual friction between parallel two-dimensional electron systems. *Physical Review Letters* **66**, 1216 (1991).
 - [3] J. P. Eisenstein and A. H. MacDonald, Bose-Einstein condensation of excitons in bilayer electron systems. *Nature* **432**, 691 (2004).
 - [4] R. V. Gorbachev, A. K. Geim, M. I. Katsnelson, K. S. Novoselov, T. Tudorovskiy, I. V. Grigorieva, A. H. MacDonald, S. V. Morozov, K. Watanabe, T. Taniguchi, and L. A. Ponomarenko, Strong Coulomb drag and broken symmetry in double-layer graphene. *Nature Physics* **8**, 896 (2012).
 - [5] J. I. A. Li, T. Taniguchi, K. Watanabe, J. Hone, A. Levchenko, and C. R. Dean, Negative Coulomb Drag in Double Bilayer Graphene. *Physical Review Letters* **117**, 046802 (2016).

- [6] K. Lee, J. Xue, D. C. Dillen, K. Watanabe, T. Taniguchi, and E. Tutuc, Giant Frictional Drag in Double Bilayer Graphene Heterostructures. *Physical Review Letters* **117**, 046803 (2016).
- [7] H. Min, R. Bistritzer, J.-J. Su, and A. H. MacDonald, Room-temperature superfluidity in graphene bilayers. *Physical Review B* **78**, 121401 (2008).
- [8] A. Perali, D. Neilson, and A. R. Hamilton, High-Temperature Superfluidity in Double-Bilayer Graphene. *Physical Review Letters* **110**, 146803 (2013).
- [9] T. Fuchs, R. Klesse, and A. Stern, Coulomb drag between quantum wires with different electron densities. *Physical Review B* **71**, 045321 (2005).
- [10] K. Flensberg, Coulomb Drag of Luttinger Liquids and Quantum Hall Edges. *Physical Review Letters* **81**, 184 (1998).
- [11] A.-P. Jauho and H. Smith, Coulomb drag between parallel two-dimensional electron systems. *Physical Review B* **47**, 4420 (1993).
- [12] A. J. Keller, J. S. Lim, D. Sánchez, R. López, S. Amasha, J. A. Katine, H. Shtrikman, and D. Goldhaber-Gordon, Cotunneling Drag Effect in Coulomb-Coupled Quantum Dots. *Physical Review Letters* **117**, 066602 (2016).
- [13] M. Yamamoto, M. Stopa, Y. Tokura, Y. Hirayama, and S. Tarucha, Negative Coulomb Drag in a One-Dimensional Wire. *Science* **313**, 204 (2006).
- [14] D. Laroche, G. Gervais, M. P. Lilly, and J. L. Reno, 1D-1D Coulomb Drag Signature of a Luttinger Liquid. *Science* **343**, 631 (2014).
- [15] M. Titov, R. V. Gorbachev, B. N. Narozhny, T. Tudorovskiy, M. Schütt, P. M. Ostrovsky, I. V. Gornyi, A. D. Mirlin, M. I. Katsnelson, K. S. Novoselov, A. K. Geim, and L. A. Ponomarenko, Giant Magnetodrag in Graphene at Charge Neutrality. *Physical Review Letters* **111**, 166601 (2013).
- [16] J. C. W. Song, D. A. Abanin, and L. S. Levitov, Coulomb Drag Mechanisms in Graphene. *Nano Letters* **13**, 3631 (2013).
- [17] S. K. Lyo, Coulomb drag between two-dimensional and one-dimensional electron gases. *Physical Review B* **68**, 045310 (2003).
- [18] A. Levchenko and A. Kamenev, Coulomb Drag at Zero Temperature. *Physical Review Letters* **100**, 026805 (2008).
- [19] Y. V. Nazarov and D. V. Averin, Current Drag in Capacitively Coupled Luttinger Constrictions. *Physical Review Letters* **81**, 653 (1998).
- [20] G. A. Fiete, K. Le Hur, and L. Balents, Coulomb drag between two spin-incoherent Luttinger liquids. *Physical Review B* **73**, 165104 (2006).
- [21] A. P. Dmitriev, I. V. Gornyi, and D. G. Polyakov, Coulomb drag between ballistic quantum wires. *Physical Review B* **86**, 245402 (2012).
- [22] M. Büttiker, Four-Terminal Phase-Coherent Conductance. *Physical Review Letters* **57**, 1761 (1986).
- [23] A. F. Croxall, K. Das Gupta, C. A. Nicoll, M. Thangaraj, H. E. Beere, I. Farrer, D. A. Ritchie, and M. Pepper, Anomalous Coulomb Drag in Electron-Hole Bilayers. *Physical Review Letters* **101**, 246801 (2008).
- [24] S. Kim and E. Tutuc, Coulomb drag and magnetotransport in graphene double layers. *Solid State Communications Exploring Graphene, Recent Research Advances*, **152**, 1283 (2012).
- [25] V. Moldoveanu and B. Tanatar, Coulomb drag in parallel quantum dots. *EPL (Europhysics Letters)* **86**, 67004 (2009).
- [26] R. Sánchez, R. López, D. Sánchez, and M. Büttiker, Mesoscopic Coulomb Drag, Broken Detailed Balance, and Fluctuation Relations. *Physical Review Letters* **104**, 076801 (2010).
- [27] A. Levchenko and A. Kamenev, Coulomb Drag in Quantum Circuits. *Physical Review Letters* **101**, 216806 (2008).
- [28] K. Kaasbjerg and A.-P. Jauho, Correlated Coulomb Drag in Capacitively Coupled Quantum-Dot Structures. *Physical Review Letters* **116**, 196801 (2016).

Coulomb drag between carbon nanotube and graphene - Supplementary information

Jean-Damien Pillet, Austin Cheng, Takashi Taniguchi, Kenji Watanabe, Philip Kim

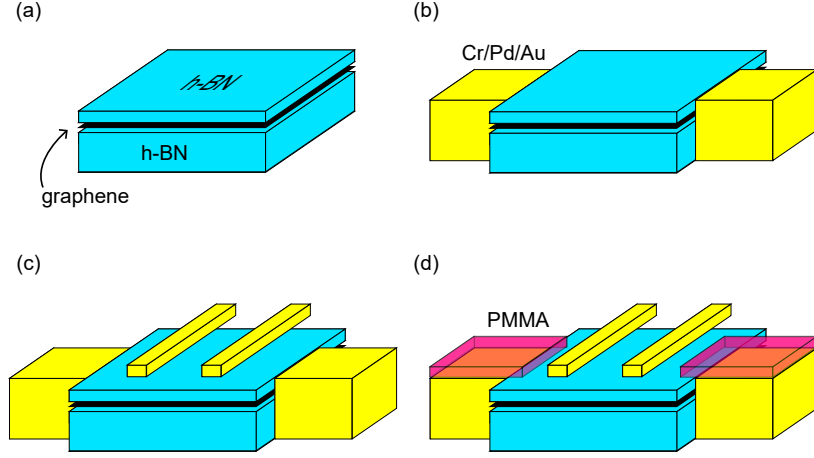


Figure S1. Sequence of preparation of the h-BN encapsulated graphene for nanotube transfer. (a) A schematic diagram depicts h-BN/graphene/h-BN encapsulated samples. (b) The graphene is electrically connected after a first step of lithography using reactive ion etching in order to expose the edges of the graphene flake followed by a metallic evaporation. (c) Electrodes, electrically isolated from the graphene by the top layer of h-BN, are fabricated for the electric connection of the carbon nanotube. (d) The sample is partially covered with PMMA resist. It will help the subsequent incorporation of a carbon nanotube in the structure.

I. FABRICATION

A. Preparation of the circuit

The sample shown in Fig. 1 of the main text is based on the initial preparation of an hexagonal boron nitride (h-BN) encapsulated graphene [1] (Fig. S1 (a)) on an n-doped silicon wafer with 285 nm SiO_2 . The thickness of the top h-BN layer is chosen between 5 and 15 nm and the bottom one around 20 nm. We use standard technique of electron beam (e-beam) lithography to design the electrodes contacting the graphene channel. We first expose the edges of the graphene encapsulated between two flakes of h-BN stack by reactive ion etching through a resist mask and subsequently evaporate a metallic trilayer Cr(1nm)/Pd(15nm)/Au(50nm) through the same mask (Fig. S1 (b)). A second step of lithography is then performed to design electrodes (same metallic trilayer) on top of the top h-BN layer. These electrodes are used to contact the carbon nanotube during the transfer step described at the end of this section (Fig. S1 (c)). The sample is covered with a 100nm thick layer of resist (PMMA A4 495K) except for areas of interest where we want the nanotube to connect electrodes during transfer. The resist will help for an efficient transfer of the carbon nanotube (Fig. S1 (d)).

B. Growth of nanotubes and characterization

Carbon nanotubes are grown and characterized following the techniques described in Ref. [2]. They are grown on $5 \times 5 \text{ mm}^2$ silicon chip with a slit in the center (see bottom of Fig. S2) using standard technique of chemical vapor deposition. A catalyst is deposited on one side of the slit (middle) such that carbon nanotubes grow suspended (top). One of these nanotubes, suspended over a slit that is $65 \mu\text{m}$ wide and 1mm long, is shown in the optical photograph of Fig. S2. It is covered with 30 nm of Au, so it can be imaged optically.

After growth, the suspended carbon nanotubes across the slits can be characterized using Rayleigh Scattering spectroscopy. This helps to identify whether nanotubes are metallic or semiconducting as illustrated in Fig. S3. Moreover it also allows the measurement of the position of the carbon nanotube along the slit such that it can be aligned with the circuit for subsequent transfer.

C. Transfer

The incorporation of the carbon nanotube into the circuit is performed by mechanical transfer [3] similarly to the method for the fabrication procedure of h-BN encapsulated graphene. The slit is placed above the circuit in order to

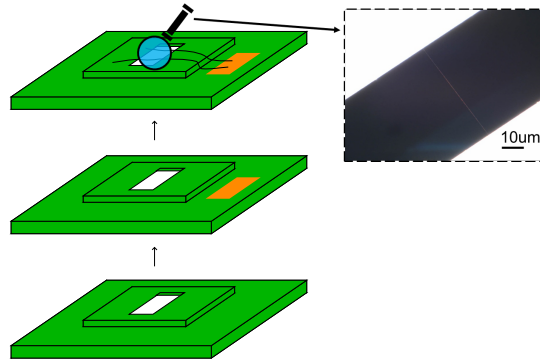


Figure S2. Sequence illustrating the growth of suspended carbon. A silicon chip with a slit (bottom) is covered with catalyst for nanotube growth (yellow). Using a standard chemical vapor deposition technique, nanotubes are grown suspended over the slit (top). The optical picture shows a suspended nanotube covered with gold such that it can be seen optically. nanotubes.

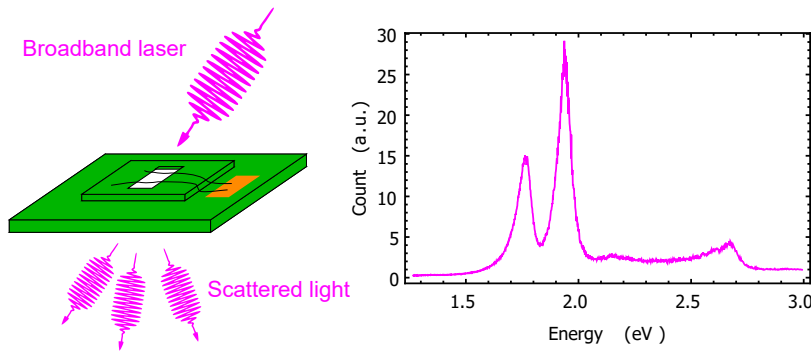


Figure S3. Rayleigh scattering. Carbon nanotubes are characterized when suspended over the slit by illumination of a broadband laser. The scattered light is collected with a detector (left). A typical Rayleigh-scattering spectrum is shown on the right. From the spectrum, we can identify the structure of carbon nanotubes. In this example the nanotube was metallic with a (16, 4) chirality.

align the nanotube with the area of interest where we have designed dedicated electrodes. The slit is pressed on the sample as shown in Fig. S4. When we have a good mechanical contact, we heat the chips up to 180°C for 5 minutes in order to melt the resist that will help the transfer of the nanotube from the slit to the target chip. The two chips are then slowly separated after they have cooled down to room temperature.

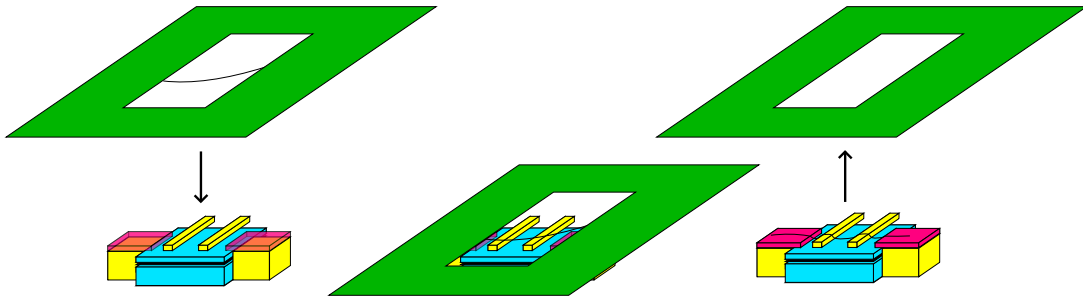


Figure S4. Sequence illustrating the nanotube transfer. The slit on which the nanotube is suspended is aligned with the h-BN encapsulated graphene (left). The slit with the characterized nanotubes is then pressed onto the target chip that is heated up to 180°C in order to melt the resist and favor the transfer of the nanotube from one chip to another (center). The two chips are then separated from each other and the nanotube is left onto its electrodes and over the h-BN/graphene/h-BN heterostructure.

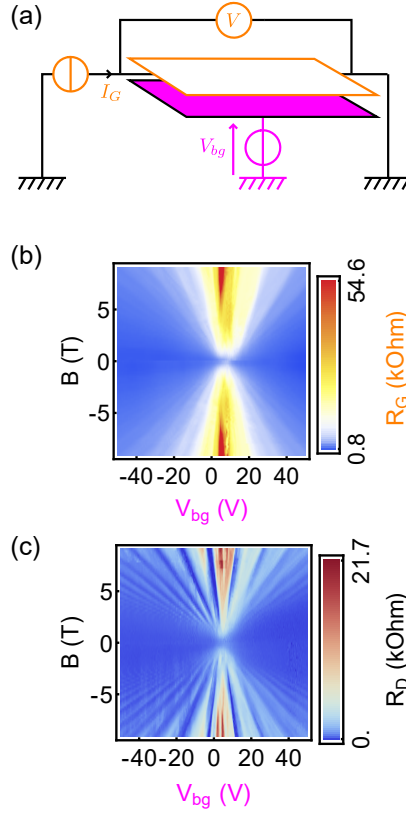


Figure S5. Onsager relation. (a) Setup for two-terminal measurement of the graphene resistance. (b) Two-terminal measurement of the graphene resistance R_G as a function of V_{bg} and B . It is symmetric with magnetic field and obeys the Onsager reciprocity relations. (c) Symmetrized drag resistance $R_D = (R_D^{NT}(B) + R_D^G(-B))/2$ obtained from data of Fig 2 (d) and (e) of the main text. It is also symmetric with B and fulfills the condition $R_D(B) = R_D(-B)$.

II. GRAPHENE MAGNETO-RESISTANCE - ONSAGER RELATION

In Fig. 2 of the main text, we present measurements of the drag resistance that are not symmetric with the applied magnetic field, *i.e.* $R_D(B) \neq R_D(-B)$. For a two-terminal measurement, such observation would imply a violation of the Onsager reciprocity relations [4] that originate from time-reversal symmetry. We can test this symmetry by measuring, for example, the two-terminal resistance of graphene R_G . This measurement is shown in Fig. S5 (a) and (b) as a function of V_{bg} and B . We can see that the measured R_G is symmetric with magnetic field.

For R_D , the conditions imposed by Onsager relations are different because we are performing a multi-terminal measurement. For the multi-terminal devices, the Onsager reciprocal relations require $R_{i,j}^{k,l}(B) = R_{k,l}^{i,j}(-B)$, where i, j and k, l are pairs of electrodes. In our drag measurement, we can symmetrize the signal and define the drag resistance as $R_D = (R_D^{NT}(B) + R_D^G(-B))/2$ where $R_D^{NT(G)}$ is the drag resistance measured across the nanotube (resp. across graphene). Fig. S5 (c) displays the symmetrized R_D as a function of V_{bg} and B .

III. CHARGE TRANSPORT IN QUANTUM DOT WITH PHENOMENOLOGICAL FRICTION FORCE

In measurements of Fig. 3 (b) shown in the main text, we observe that charge states in the nanotube modulated by back gate voltage can dramatically affect the out-of-equilibrium drag in the configuration where one electrode is grounded (and the other one is floating with a potential V_{NT} (Fig. 3 (c, d)). This behavior can be described by a phenomenological model where the nanotube is modeled as a quantum dot and the electrons that it contains experience a dragging friction force due to the presence of a current underneath it in the graphene channel. This force, proportional to the current I_G flowing in the graphene channel, can be written $\vec{F}_f = \eta_{eff} I_G \vec{u}_{NT}$ where η_{eff} is an effective friction coefficient and \vec{u}_{NT} is a unitary vector along the carbon nanotube oriented in the positive direction of I_G . This friction force can displace electrons between the grounded electrode and the floating one (Fig. 3 (c) and

(d)) and therefore affect the potential V_{NT} and the average number of charge n_{NT} in the nanotube. If the distance between the source and drain electrodes connecting the nanotube is L , then the work W_F of the friction force when an electron is transferred from source to drain is

$$W_F = \eta_{eff} I_G L$$

Assuming the device is approximately symmetric, an electron that stops in the nanotube will acquire energy $W_F/2$ because it travels only half the distance.

When no current is flowing through the graphene, the whole system is at equilibrium with n_0 charge in the nanotube (controlled by the back gate with a leverage α) and a potential $V_{NT} = 0$ on the floating electrode. If $I_G \neq 0$, then the system is driven out-of-equilibrium. Consequently, a given number of electron N is transferred from the grounded electrode to the floating electrode while the average number of charge in the nanotube changes by an amount $\delta n_{NT} = n_{NT} - n_0$, where n_{NT} is the number of electrons in the nanotube and n_0 is n_{NT} at equilibrium. The potential of the floating electrode V_{NT} therefore becomes finite. Again if we assume that the device is approximately symmetric, the potential of the nanotube changes $\sim V_{NT}/2$. Considering all the above contributions, the energy of the whole system thus increases by

$$\Delta E(N, \delta n_{NT}) = -e(N \times V_{NT} + n_{NT} \times V_{NT}/2) + (N \times W_F + \delta n_{NT} \times W_F/2) + \frac{e^2}{2C_{NT}} \left[(n_{NT} - \alpha V_{bg})^2 - (n_0 - \alpha V_{bg})^2 \right]$$

where the first term is the change of electrostatic energy due to the increase of V_{NT} , the second is the work from friction, and the third one is the variation of charging energy of the nanotube, C_{NT} being the capacitance of the nanotube. Here, we have neglected the charging energy of the floating electrode since its capacitance (hundreds of fF, essentially due to the wiring) is typically 3 orders of magnitude large than C_{NT} (hundreds of aF).

For a given I_G , the minimum energy of the system is reached for $\partial \Delta E / \partial \delta n_{NT} = 0$, which leads to the equality

$$V_{NT} = \frac{\eta_{eff} L}{e} I_G + 2e \frac{\delta n_{NT}}{C_{NT}} \quad (S1)$$

Since the drag resistance is given by $R_D = \partial V_{NT} / \partial I_G$, we can introduce a constant $R_D^0 = \eta_{eff} L / e$, which is the drag resistance if we neglect the charge fluctuations. In Fig. 3 (b), R_D^0 corresponds to R_D measured at $I_G = 0$ and is approximately equal to 125Ω for this range of V_{bg} in this measurement.

The role of δn_{NT} can be incorporated modeling the carbon nanotube as a quantum dot with a single orbital of energy ϵ , tunable linearly with V_{bg} , relative to the Fermi energy of the electrodes. We consider here the simplest case of a single energy level with a sufficiently large charging energy $e^2/2C_{NT}$ such that this orbital can only be unoccupied or singly occupied, with a small symmetric coupling $\Gamma \ll k_B T$ to the two electrodes, where k_B is the Boltzmann constant and T the temperature. Under these conditions, one can calculate the average charge in the quantum dot by solving the master equations of the system [5]

$$\delta n_{NT} = \frac{1}{2 \left(\exp \left(\frac{\mu_{NT} - \mu_L}{k_B T} \right) + 1 \right)} + \frac{1}{2 \left(\exp \left(\frac{\mu_{NT} - \mu_R}{k_B T} \right) + 1 \right)} \quad (S2)$$

where $\mu_{NT} = \epsilon - eV_{NT}/2$, $\mu_L = -eV_{NT}$ and $\mu_R = 0$. In principle, one should solve the problem self-consistently by combining Eq. S1 and S2. For simplicity, we calculate V_{NT} to the first order in the variation $\delta n_{NT} \ll 1$, taking $\mu_L \approx -W_F$ and $\mu_{NT} \approx \epsilon - W_F/2$. We obtain the simulated drag resistance shown in Fig. 3 of the main text where $R_D^0 = 125 \Omega$, $C_{NT} = 100$ aF and $T = 1.6$ K were chosen for experimental parameters to produce a reasonable agreement with our experimental observations. This value of C_{NT} is consistent with the typical charging energy that we observe (a few meV), though slightly underestimated. Fig. S6 shows that δn_{NT} can be controlled with the back gate ($\epsilon \propto -V_{bg}$) and also with the current I_G flowing through graphene.

Similarly, we can calculate the conductance of the nanotube G_{NT} using the master equation formalism. Here, one electrode on the nanotube is grounded and the other one is connected to a voltage source at a voltage V_{bias} . Then, the current flowing through the nanotube for $I_G = 0$ is given by

$$I_{NT} = \frac{4e\Gamma}{h} \left[\frac{1}{\left(\exp \left(\frac{\epsilon_0 - eV_{bias}/2}{k_B T} \right) + 1 \right)} - \frac{1}{\left(\exp \left(\frac{\epsilon_0 + eV_{bias}/2}{k_B T} \right) + 1 \right)} \right]$$

where Γ is the coupling constant of the electrodes to the nanotube channel. From this equation, the nanotube conductance is given by $G_{NT} = \partial I_{NT} / \partial V_{bias}$. Shown in Fig. 3 (g) is the calculation of G_{NT} , obtained for $\Gamma \approx k_B T$. In Fig. S7, we can see that G_{NT} is peaked when the Fermi level of source or drain is aligned with ϵ as expected.

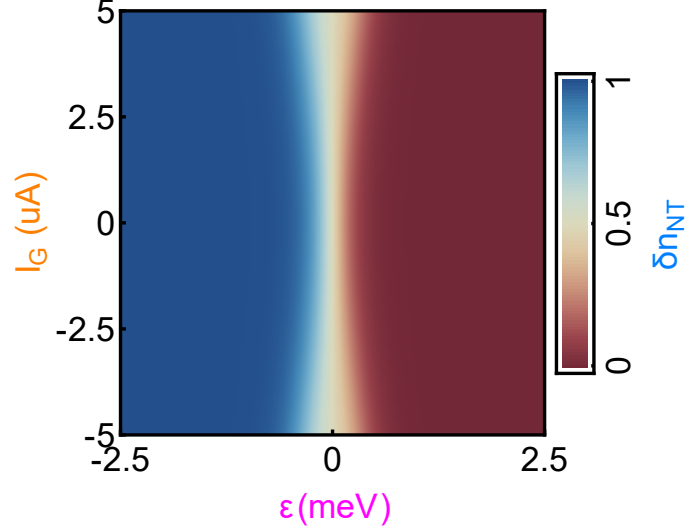


Figure S6. Calculation of charge fluctuations calculated from Eq. S2. The charge variation δn_{NT} in the quantum dot is controlled by the back gate that controls the energy of the orbital ϵ . The current flowing through the graphene can also induce modulation of δn_{NT} . As I_G increases, the region where δn_{NT} remains close to 0.5 expands (white area).

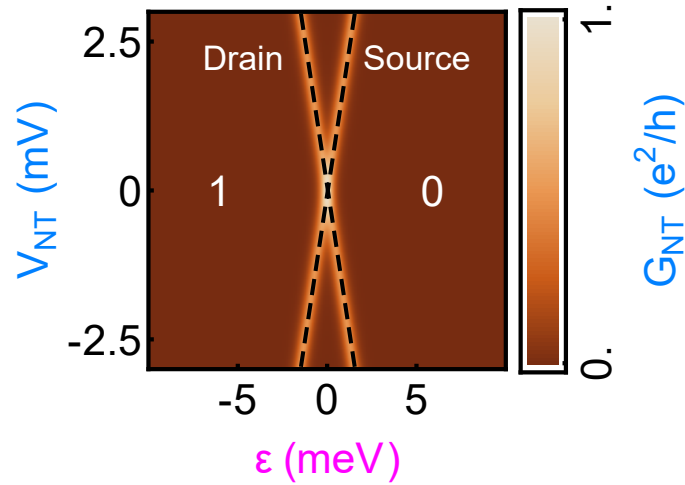


Figure S7. Calculation of electrical conductance through a carbon nanotube quantum dot as a function of the bias voltage and single electron energy level. Parts of Coulomb diamonds are shown, where the conductance enhancement due to alignment of a nanotube electronic level with Fermi levels of source or drain electrodes is apparent at the boundaries of the diamonds (marked by dashed lines). The number of charge n_{NT} is indicated in each diamonds.

IV. LINEAR LUMPED ELEMENT ANALYSIS AND SETUP FOR SIMULTANEOUS MEASUREMENT OF G_{NT} AND R_D

A. Setup for simultaneous measurement of G_{NT} and R_D

Measurements presented in Fig. 4 of the main text are obtained by applying voltages at the same time on nanotube (V_{NT}) and graphene (V_G). This way, we can measure current I_{NT} through the nanotube with two components: a standard resistive contribution due to V_{NT} and a drag contribution due to V_G . We can distinguish these two contributions by frequency-division multiplexing using the setup of Fig. S8 with voltages having both a DC and an AC part and using two lock-in amplifiers set at different frequencies f_{NT} and f_G , for V_{NT} and V_G , respectively.

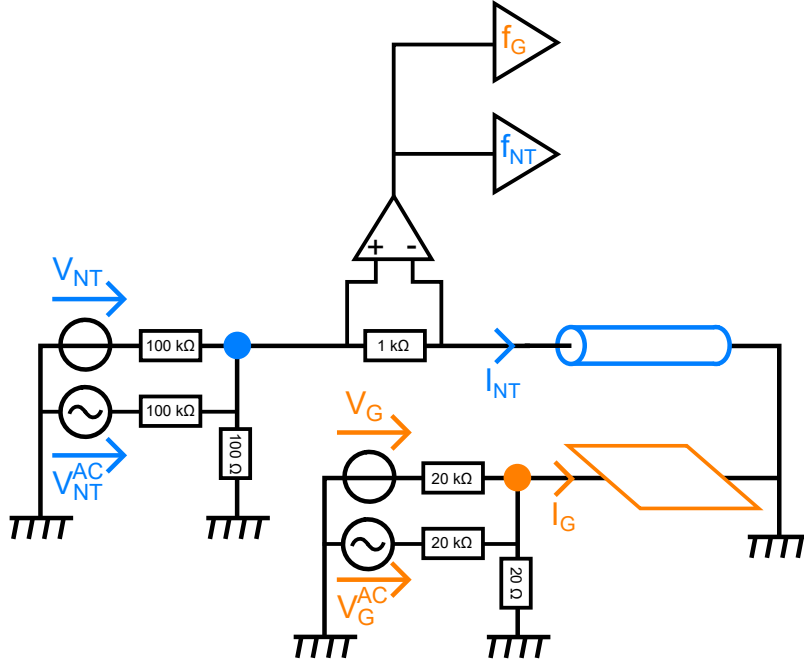


Figure S8. Setup for simultaneous measurement of G_{NT} and R_D . Voltages are applied across the nanotube and graphene. Using voltage dividers, AC and DC parts are summed such that on the blue (orange) spot the total voltage that is applied is $V_{NT}^{tot} = (V_{NT} + V_{NT}^{AC} \cos(2\pi f_{NT}t)) / 1000$ ($V_G^{tot} = (V_G + V_G^{AC} \cos(2\pi f_Gt)) / 1000$). Using a differential voltage amplifier, we measure the current I_{NT} flowing through the nanotube that we deduce from the voltage across a resistance of $1\text{ k}\Omega$, negligible compared to R_{NT} , in series with the nanotube. Two lock-in amplifiers are measuring at frequencies f_G and f_{NT} the differential conductance of the nanotube G_{NT} and the differential drag conductance σ_D .

B. Linear lumped element analysis

Right most plot of Fig. 4 (c) of the main text shows measurements of R_D as a function of voltages applied across the nanotube V_{NT} and the graphene channel V_G (see Fig. 4 (a)). In this configuration, none of the electrodes are floating, and thus uncontrolled charge fluctuations are suppressed. In this out of equilibrium transport regime, R_D can be modulated by both V_{NT} and V_G , whose contributions can even oppose each other, resulting in negative R_D in certain experimental conditions. It is instructive to perform a linear lumped element analysis of the device in order to understand the origin of the negative differential resistance.

The simplest description of the charge drag is to consider the nanotube (resp. the graphene) as a voltage source whose electromotive force $R_D I_G$ (resp. $R_D I_{NT}$) is driven by the current flowing in the graphene (resp. nanotube). This source has a series resistance corresponding to the resistance of the nanotube R_{NT} (resp. graphene R_G) in absence of drag. The configuration of Fig. 4 (a) is thus equivalent to the schematic of Fig. 4 (b), from which we can write

$$\begin{cases} V_{NT} - R_D I_G &= R_{NT} I_{NT} \\ V_G - R_D I_{NT} &= R_G I_G \end{cases}$$

If we combine these two coupled equations, we find that

$$I_{NT} = \frac{R_G}{R_{NT} R_G + R_D^2} \left[V_{NT} - \frac{R_D}{R_G} V_G \right]$$

In our experiment, $R_D, R_G \ll R_{NT}$, and we obtain

$$\begin{cases} \partial I_{NT} / \partial V_{NT} &\approx 1 / R_{NT} \\ \partial I_{NT} / \partial V_G &\approx R_D / R_G R_{NT} \end{cases}$$

From the first equation we obtain $G_{NT} = 1 / R_{NT}$. From the second equation, we can define the differential drag conductance σ_D . Note that σ_D is related to the drag resistance using the relation $R_D = \sigma_D R_G R_{NT}$.

Using the analysis provided above, we now can also identify regions where currents in the nanotube and graphene are in similar or opposite directions. If we set $I_G = 0$, we obtain $V_G = R_D/R_{NT}V_{NT}$. Therefore, if $V_G > R_D/R_{NT}V_{NT}$ (resp. $V_G < R_D/R_{NT}V_{NT}$), then $I_G > 0$ (resp. $I_G < 0$). Since $R_D \ll R_{NT}$, this limit is roughly $V_{NT} \approx 0$. Similarly, if we set $I_{NT} = 0$, we obtain $V_{NT} = R_D/R_GV_G$. Using these relations, we can identify where I_{NT} is positive or negative. These two boundaries are represented by the dotted lines in Fig. 4 (c) of the main text.

-
- [1] L. Wang, I. Meric, P. Y. Huang, Q. Gao, Y. Gao, H. Tran, T. Taniguchi, K. Watanabe, L. M. Campos, D. A. Muller, J. Guo, P. Kim, J. Hone, K. L. Shepard, and C. R. Dean, *Science* **342**, 614 (2013).
 - [2] M. Y. Sfeir, F. Wang, L. Huang, C.-C. Chuang, J. Hone, S. P. O'Brien, T. F. Heinz, and L. E. Brus, *Science* **306**, 1540 (2004).
 - [3] X. M. H. Huang, R. Caldwell, L. Huang, S. C. Jun, M. Huang, M. Y. Sfeir, S. P. O'Brien, and J. Hone, *Nano Letters* **5**, 1515 (2005).
 - [4] L. Onsager, *Physical Review* **37**, 405 (1931).
 - [5] C. W. J. Beenakker, *Physical Review B* **44**, 1646 (1991).